Functionality by Nanostructuring: PECVD of Tin-Sulfide Nanowalls

C. Ruhmlieb[1], M. Taplick[1], C. Strelow[1], T. Kipp[1] and A. Mews[1]

[1]*Institute of Physical Chemistry, University of Hamburg, Hamburg, Germany*

Abstract: Orthorhombic tin sulfide features anisotropic electric properties, i.e. an enhanced electron mobility along the van-der-Waals gap between two SnS layers. By nanostructuring, this anisotropy can be utilized to improve the performance of SnS as absorber in solar cells. We report on the large-area deposition of vertically aligned, phase-pure SnS nanowalls via PECVD using a metal-organic single-source precursor. Optical-emission spectroscopy gives insight into the precursor fragmentation. Via simple *I-V* curve measurements, we demonstrate the significantly enhanced conductivity of vertically aligned SnS nanowalls.

Keywords: PECVD, MOCVD, SnS, nanowalls, anisotropy.

1. Introduction

Tin(II)sulfide (α-SnS) is a non-toxic, earth-abundant IV-VI p-type semiconductor, that naturally crystallizes two-dimensionally [1]. The layered orthorhombic crystal structure is shown in Figure 1. As a consequence of the van-der-Waals gap between two layers, the electron mobility in [001] direction is many times higher than in the other directions of the crystal. The anisotropic crystal growth leads to anisotropic electronic properties. The band gap of 1.3 eV hits the maximum of the solar spectrum [2], so that SnS is discussed as a highly promising absorber material for solar cells. Nevertheless, the highest reported efficiency for tin-sulfide based solar cells does not exceed 5% [3].

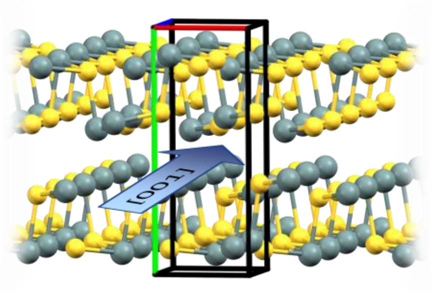

Fig. 1. Layered crystal structure and unit cell of orthorhombic α-SnS with illustrated direction of enhanced electron mobility in [001] direction.

In order to overcome efficiency limitations and to exploit the tremendous potential of tin sulfide as absorber layer, the idea is to take advantage of the electron fast track by directed, vertical growth of tin-sulfide nanosheets along [001]. A morphology that is known from carbon nanowalls [4] is aspired. Hence, the direction of the electric anisotropy would follow the vertical geometry of the solar cell, leading to a decreased recombination probability of the photo-generated charge carriers. Consequently, the efficiency of SnS-based solar cell might be increased by using SnS nanowalls, instead of undirected SnS layers.

2. Single-Source Precursor

For the PECVD of SnS nanowalls, a tin-organic single-source precursor was synthesized via a simple precipitation reaction of $SnCl_2 \cdot 2H_2O$ and $Na(dedtc) \cdot 3H_2O$ in water. The resulting yellow powder was analysed with regard to the elemental composition, crystalline structure and thermal decomposition behaviour. Applying ^{119}Sn-MAS NMR spectroscopy revealed that the main compound of the precursor powder is bis(diethyldithiocarbamato)tin(II) ($[Sn(dedtc)_2]$), sketched in Figure 2, accompanied by $[S_2Sn_2(dedtc)_4]$ and $[Sn(dedtc)_4]$. Thermogravimetric analysis of the precursor powder shows a one-step weight loss at approx. 250 °C that can be correlated to the evaporation of $Sn(dedtc)_2$.

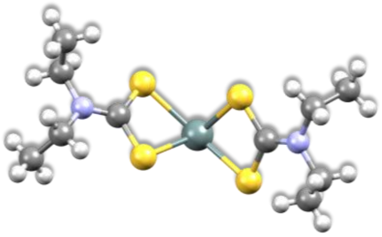

Fig. 2. Ball-and-stick model of $Sn(dedtc)_2$ constructed from single-crystal diffraction data.

3. Optical Emission Spectroscopy

In-situ optical emission spectroscopy (OES) of the plasma gives insight into plasma processes during the SnS deposition. For this, we recorded emission spectra of the Ar/N_2 plasma before and during the deposition. Additional signals occur when the precursor reaches the plasma. Actually, all signals can be accurately assigned to atomic and molecular species originating from the tin-organic compounds, e.g., S^{II} and NCS species. Moreover, the relative intensities of the additional signals stay constant over the reaction time, which fits to the observation that $Sn(dedtc)_2$ shows a sublimation behaviour upon thermal treatment. Thus, tin and sulfur are released when the precursor is decomposed by plasma impact. Two-dimensional spectroscopic plasma mapping allows the identification of hot spots in the reaction zone. For this, the plasma region is raster scanned in 100x60 pixels and for each pixel an optical emission spectrum has been recorded. The recorded information can be translated, e.g., into spatially resolved plasma-intensity maps, as shown in Figure 3, or in electron-temperature maps.

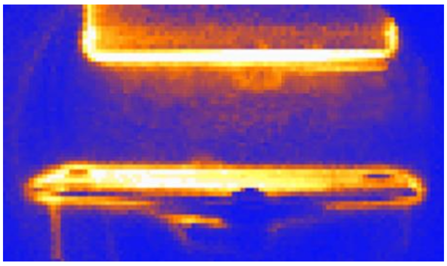

Fig. 3. Plasma-intensity map of the reaction chamber.

4. PECVD of SnS Nanowalls

SnS nanowalls were synthesized on metal-covered Si/SiO_2 [100] wafer substrates using a home-built PECVD setup (CCP, 13.56 MHz). Depending on the synthetic parameters, the morphology of the deposited tin sulfide can be tailored from stacks to thin vertically aligned nanosheets (Fig. 4). X-Ray diffraction analysis proves that the deposited structures are phase-pure orthorhombic α-SnS. Moreover, since texture effects are changing relative reflex intensities of the XRD pattern, they give information about the crystal orientation of the nanowalls. Investigating detached nanosheets via transmission electron microscopy and electron diffraction shows that the nanowalls actually grow along [001]. This should thus enable a fast electron transport in vertical direction. The absence of organic species was confirmed via energy-dispersive X-Ray spectroscopy.

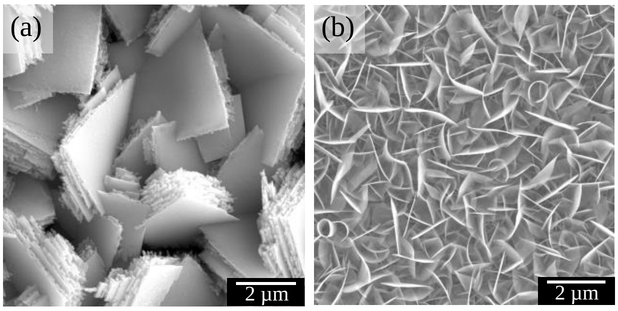

Fig. 4. SEM images of PECVD-grown (a) SnS stacks and (b) thin SnS nanowalls.

It turned out that the shape of the SnS structures strongly depends on the very early processes of the deposition, i.e. the interaction of the substrate surface and the plasma-activated species. We demonstrate the crucial factors for vertical crystal growth, including the role of crystal facets, surface roughness, dewetting of the substrate coverage, and catalytic processes on the contact surface between wafer and reactants.

5. Conductivity Measurements

The PECVD-grown SnS nanostructures were further characterized with regard to their electronic properties by performing *I-V* curve measurements. Since the extraordinary surface-to-volume ratio goes along with a very high surface roughness, common contacting techniques are not appropriate. Instead, we placed mercury droplets, set and contacted by stainless-steel cannulas, on the nanostructured surface. The potential was swept between ± 5 V and the resulting current was measured. As shown in Figure 5, the *I-V* curve of the SnS stacks shows a slight bending around the ordinate origin. This is due to the Schottky-type contact between mercury and SnS. Taking the geometry of the conducting channel into account, a specific conductivity of approx. 26 S/m can be calculated for the SnS stacks. In comparison, the SnS nanowalls show a much higher absolute current at ± 5 V, indicating a higher conductivity. Also the curve bending is stronger. This might be due to quantization effects. The Bohr-exciton radius of SnS is 7 nm [5], so that quantization effects can appear at a crystal thickness of 14 nm and less. In this case, an increased band gap would result in an increased Schottky barrier, leading to a stronger bending of the characteristic curve. A specific conductivity of 263 S/m was calculated, assuming an active contact area between mercury droplet and nanowalls of 20%.

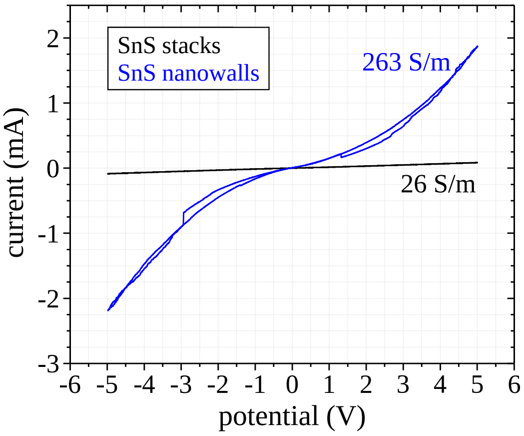

Fig.5. *I-V* curves of SnS stacks (black) and SnS nanowalls (blue) at ambient conditions.

The *I-V* curves demonstrate a strongly enhanced electric conductivity of the vertically aligned SnS nanowalls, indicating a more efficient charge-carrier transport along the [001] plane.

6. Conclusions

We achieved a large-area deposition of vertically aligned SnS nanowalls by a modified PECVD technique. For this, bis(diethyldithiocarbamato)tin(II) was used as solid single-source precursor that is decomposed by plasma impact. Optical emission spectroscopy gives information about the precursor fragmentation. The morphology of the phase-pure α-SnS structures can be influenced by substrate temperature and substrate coverage. Finally, the deposited structures showed an enhanced specific conductivity.

7. References

[1] M.M. Kobylinski, C. Ruhmlieb, A. Kornowski, A. Mews, J. Phys. Chem. C, **122**, 10, (2018).
[2] N.P. Dasgupta, X. Meng, J.W. Elam, A.B.F. Martinson, Acc. Chem. Res., **48**, (2015).
[3] P. Sinsermsuksakul, L. Sun, S.W. Lee, H.H. Park, S.B. Kim, C. Yang, R.G. Gordon, Adv. Energy Mater., **4**, 15, (2014).
[4] M. Höltig, C. Ruhmlieb, C. Strelow, T. Kipp, A. Mews, Z. Phys. Chem, **229**, (2015).
[5] G.H. Yue, L.S. Wang, Y.Z. Chen, D.L. Peng, Nanoscale Res. Lett., **4**, (2009).